Check for updates

[Sn₃OF]PO₄ vs. [Sn₃F₃]PO₄: enhancing birefringence by breaking the R3 symmetry and realigning lone pairs†

Yuhan Hu,[a,b] Xi Xu,[a] Ruixi Wang,[b] Jingyun Han,[a] Shunsong Zhang,[a] Shuhui Zhan,[a] Jingyu Guo,*[a,b] Li-Ming Wu [ID] *[a,b] and Ling Chen [ID] *[a,b]

Tin(II)-containing phosphates are promising candidates for designing and studying materials with enhanced birefringence. Herein, we present a novel compound [Sn₃OF]PO₄ that exhibits significant birefringence ($\Delta n_{obv.}$ = 0.117 at 546 nm), a five-fold improvement compared to that of the related compound [Sn₃F₃]PO₄ discovered nearly 40 years ago. The remarkable enhancement in birefringence is primarily attributed to the anisotropic [SnO₃F]⁵⁻ structure building unit. By simple regulation of the F/O ratio, the undesirable R3 symmetry in [Sn₃F₃]PO₄ is disrupted. This regulation also realigns the lone pairs, resulting in substantial optical anisotropy.

10th anniversary statement

Congratulations on the 10th anniversary of ICF! These 10 years of ICF coincide with the second decade of my personal research career. As a founding member of the ICF editorial board, I have been actively involved in the forums organized by ICF.

Over the past decade, my collaborator Li-Ming Wu and I at BNU have made significant progress in the field of inorganic solid-state chemistry. We have explored the design and synthesis of novel compounds, studied the relationship between properties and crystal structures (focusing primarily on nonlinear optical and thermoelectric properties), and found ways to modify and enhance these properties.

Thank you for being with me throughout this journey!

Introduction

Birefringence (Δn) is a phenomenon that manifests in anisotropic media, particularly in non-cubic crystals.[1–4] It reflects the optical anisotropy of a crystal, which is one of the essential properties of optoelectronic functional crystals. A crystal with an appropriate birefringence is a crucial component of all-solid-state lasers, as it can modulate the polarized light for a single wavelength laser output. In fact, the birefringence phenomenon originates from the structural anisotropy of crystals. Therefore, effective and significant approaches are employed for enhancing birefringence to increase the anisotropy of the structure building units and optimize the arrangement in the crystal structure.

At present, there are several main methods to increase birefringence.[5–8] Firstly, introducing anisotropic building units (ABUs) with large birefringence is an effective approach for designing birefringent crystals, such as $[BO_3]^{3-}$, $[NO_3]^-$, $[CO_3]^{2-}$, $[C_4O_4]^{2-}$, and $[C_3N_3O_3]^{3-}$.[5,6] Secondly, to broaden the

[a]*Center for Advanced Materials Research, Beijing Normal University, Zhuhai 519087, People's Republic of China*
[b]*Beijing Key Laboratory of Energy Conversion and Storage Materials, College of Chemistry, Beijing Normal University, Beijing 100875, People's Republic of China*

5648 | *Inorg. Chem. Front.*, 2024, **11**, 5648–5656

This journal is © the Partner Organisations 2024

range of available ABUs, a novel approach has recently emerged: designing ABUs by encompassing diverse chemical bonds (ABUCBs), which has garnered interest among researchers.[9] The incorporation of ABUCBs into the crystal structure is likely to induce anisotropy in both the crystal structure and the spatial electron distribution. The latest experimental advancements indicate, for instance, that the introduction of P–F or B–F bonds enhances microscopic polarization anisotropy and hyperpolarization, eventually resulting in improved macroscopic properties, such as Δn.[10–18] Thirdly, the utilization of stereochemically active lone pairs could effectively increase the structural anisotropy, leading to a substantial Δn enhancement.[19–23] For instance, cations such as Pb^{2+}, Sn^{2+}, Sb^{3+}, and Bi^{3+}, serving as coordination centres, constitute the ABUs. For example, $BaSn_2(PO_4)_2$ exhibits a high $\Delta n_{cal.}$ of 0.071,[19] while $Sn_2B_5O_9Cl$ demonstrates a $\Delta n_{obv.}$ of 0.168.[20]

Tin-based phosphates are excellent candidates for studying crystals with large birefringence. For example, Sn_2PO_4I[24] exhibits the largest $\Delta n_{obv.}$ of ≥ 0.664 at 546 nm among the reported borates and phosphates to date. However, the presence of Sn^{2+} with stereochemically active lone pairs does not always lead to an increase in Δn. In particular, in high-symmetry crystal structures, Δn values are typically very small, as observed in compounds like $KSn_4(PO_4)_3$[25] ($R3c$, 0.013), $NaSn_4(PO_4)_3$[26] ($R3c$, 0.005) and $[Sn_3F_3]PO_4$[27] ($R3$, 0.011).[9,28–30] In these compounds, the Sn^{2+} ions are located along the $C3$ or 3_1 axes, forming a highly symmetric ABU arrangement that does not exhibit large anisotropy. We consider that in Sn^{2+}-containing phosphates, the orientation of lone pairs plays a crucial role in determining the birefringence. However, controlling this orientation remains a challenge.

Herein, we report a novel compound, $[Sn_3OF]PO_4$, obtained by a conventional hydrothermal synthesis method. Interestingly, this compound, together with $[Sn_3F_3]PO_4$[27] known for about 40 years, provides a compelling example demonstrating that a straightforward regulation of the F/O ratio leads to a remarkable five-time enhancement of $\Delta n_{obv.}$ (0.117 *vs.* 0.027 at 546 nm). Furthermore, we delve deeper into how this simple regulation effectively disrupts the $R3$ high symmetry of the latter compound, causing all lone pairs to align consistently along the dielectric axis. As a result, a significant enhancement in birefringence is achieved. We believe that this strategy may offer new experimental guidelines for searching and designing effective birefringent crystals.

Experimental section

Synthesis of compounds

Reagents including NH_4HF_2 (Aladdin, 98%), $CO(NH)_2$ (Aladdin, 98%), SnF_2 (Bidepharm, 99%), H_3PO_4 (Aladdin, 99%), P_2O_5 (Aladdin, 99%) and B_2O_3 (Aladdin, 99.9%) were used as purchased.

Colourless block-like crystals of $[Sn_3OF]PO_4$ are obtained by hydrothermal synthesis. The raw materials, $(NH_4)_2PO_3F$,

SnF_2 and B_2O_3, were well ground in a ratio of $1:2:4$ and then put into PTFE pouches. The pouches were then enclosed in 1 mL autoclaves with PTFE inner linings, with addition of a little deionized water, and heated at 190 °C for 4 days. The pouches were cooled to room temperature at 0.5 °C min^{-1}. After cleaning with deionized water and alcohol, colorless block-like crystals were obtained. The yield of the $[Sn_3OF]PO_4$ product could not be calculated, because it is obtained by hydrothermal synthesis along with impurities, which cannot be separated.

The polycrystalline powder of $[Sn_3OF]PO_4$ is prepared by solid state synthesis. The raw materials, SnO, SnF_2 and P_2O_5, were well ground in a ratio of $5:1:1$ and then loaded into a tidy silica tube (Φ 10 mm × 100 mm) washed with deionized water and dried at a high temperature to remove the impure phases, and then the tube was flame-sealed under 10^{-3} Pa. The tube was heated to 400 °C in 3 h and held at this temperature for 4 days. Afterwards, it was cooled slowly to 250 °C at a rate of 1.0 °C h^{-1} and then cooled to room temperature quickly. Finally, the polycrystalline powder of $[Sn_3OF]PO_4$ is obtained and the yield is 100% without impurity.

In order to compare the birefringence and other optical performance, we have also synthesized $[Sn_3F_3]PO_4$ according to the literature,[27] and block-like colorless crystals and polycrystalline powders were obtained.

Single crystal X-ray diffraction and powder XRD analysis

A Bruker D8 Quest diffractometer with Mo Kα radiation (λ = 0.71073 Å) was used to collect the single-crystal X-ray diffraction (XRD) data at room temperature, and the data were integrated using the SAINT program.[31] The direct methods and the SHELXTL system[32] were used to solve and refine the crystal structure, respectively. All the atom positions were refined using full-matrix least-squares techniques. The purity of the sample was confirmed by powder XRD, which was performed on a Bruker Model D8 Advance diffractometer equipped with Cu Kα radiation at room temperature. The diffraction patterns were recorded with the 2θ range from 10 to 70°, the scanning step width was 0.02° and the scanning rate was 1 s per step. The simulated and experimental powder X-ray diffraction peaks of $[Sn_3F_3]PO_4$ and $[Sn_3OF]PO_4$ are consistent, ensuring the purity of the sample (Fig. S1†).

UV diffuse-reflectance spectroscopy

The UV-Vis-NIR diffuse reflectance spectra for $[Sn_3F_3]PO_4$ and $[Sn_3OF]PO_4$ were characterized using a Shimadzu UV-3600i Plus UV-Vis-NIR spectrophotometer at room temperature. The reflectance spectrum was transformed to absorbance using the Kubelka–Munk function.[33]

Infrared (IR) spectroscopy

Infrared (IR) spectra were recorded on a Thermo Scientific Nicolet iS50 FT-IR spectrophotometer in the range from 500 to 2000 cm^{-1} with a resolution of 1 cm^{-1}. The sample was mixed thoroughly with 500 mg of dried KBr.

This journal is © the Partner Organisations 2024

Inorg. Chem. Front., 2024, **11**, 5648–5656 | **5649**

Birefringence measurement

The refractive index differences of $[Sn_3F_3]PO_4$ and $[Sn_3OF]PO_4$ were characterized using a polarizing microscope (ZEISS Axis Scope. 5 pol) equipped with a Berek compensator. The average wavelength of the light source was 546 nm. The formula for calculating the birefringence is as follows:

$$R = |N_g - N_p| \times d = \Delta n \times d \qquad (1)$$

where R represents the optical path difference; N_g, N_p and Δn mean the refractive index of fast light, that of slow light, and the difference value of the refractive index, respectively; and d denotes the thickness of the crystal.

Thermal analysis

A NETZSCH STA 449F5 instrument was used to examine the thermal stability of $[Sn_3F_3]PO_4$ and $[Sn_3OF]PO_4$ under static N_2 conditions. The sample and reference (Al_2O_3) were encapsulated in a Pt crucible, which was heated up to 800 °C at a rate of 10 °C min^{-1} and then cooled to room temperature.

DFT calculations

Density functional theory[34,35] (DFT) calculations on the electronic structures and linear optical properties of $[Sn_3F_3]PO_4$ and $[Sn_3OF]PO_4$ were carried out using the Vienna Ab initio Simulation (VASP) Package.[36,37] The projector augmented wave (PAW) method was used to treat the valence–core interactions. The $5s$ and $5p$ states of Sn atoms, the $3s$ and $3p$ states of P atoms, the $2s$ and $2p$ states of O atoms, and the $2s$ and $2p$ states of F atoms were treated as valence states. The kinetic energy cutoff of the plane wave basis was set to be 500 eV. The Perdew–Burke–Ernzerhof[38,39] (PBE) functional within the generalized gradient approximation (GGA) was chosen to account for exchange–correlation effects. The Brillouin zone was sampled using a Gamma-centered mesh with a minimum spacing of 0.4 Å^{-1} between k points. The convergence criterion for self-consistent field (SCF) iterations and structural relaxation was set to be 10^{-6} and 10^{-5} eV, respectively. The frequency-dependent dielectric matrix was calculated using the summation-over-states approach, and then linear optical properties, including the refractive index n and the birefringence Δn, can be assessed accordingly. Recognizing the inherent underestimation of band gaps by GGA, a scissor value was applied to align calculated and experimental band gaps. The refractive indices along the crystallographic axes n_a, n_b and n_c, as well as n_x, n_y and n_z along the dielectric axes, were calculated using the ellipsoid formula, with the aid of included angles between the dielectric and crystallographic axes.

Results and discussion

Crystal structure description and comparison

$[Sn_3OF]PO_4$ is first reported herein and crystallizes in the monoclinic space group $P2_1/c$ (no. 14), with $a = 4.8865(2)$ Å, $b = 11.4484(5)$ Å, $c = 11.9947(5)$ Å, $\beta = 97.286(1)°$, $V = 665.60(5)$ Å^3,

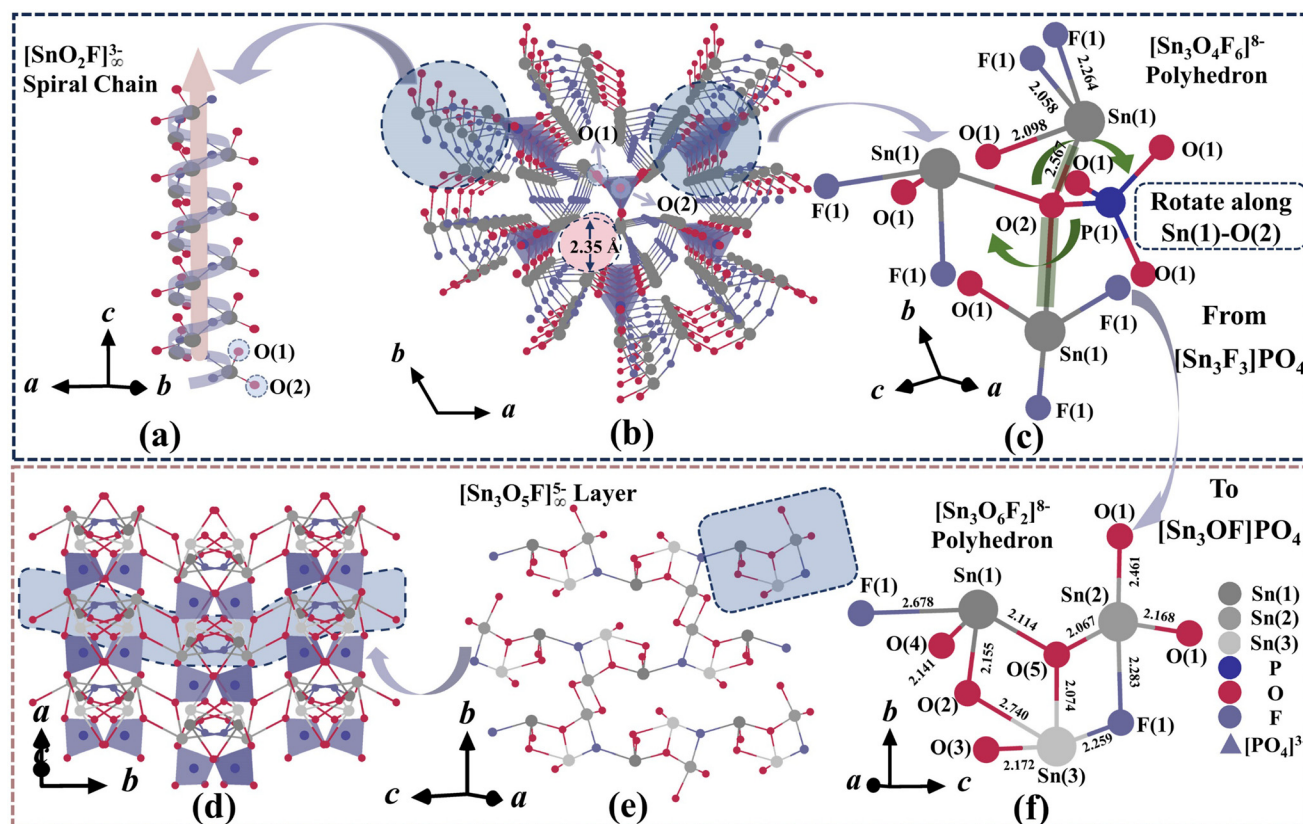and $Z = 4$ (Fig. 1 and Tables S1–S3†). Another related yet different compound established nearly 40 years ago,[27] $[Sn_3F_3]PO_4$, crystallizes in a higher symmetry trigonal space group $R3$ (no. 146), with $a = 11.8537(3)$ Å, $c = 4.6271(2)$ Å, $V = 563.05(4)$ Å^3, and $Z = 3$. Herein, the crystallographic asymmetric unit consists of one unique 9b site occupied by Sn, one unique 3a site occupied by P, one unique 9b site and one unique 3a site occupied by O and one unique 9b site occupied by F in $[Sn_3F_3]PO_4$, respectively. Because the P(1) atom is located on the triad axis, an independent P(1) and O(1) and O(2) atoms form a C_3 $[PO_4]^{3-}$ tetrahedron. There are three same P(1)–O(1) bonds with a length of 1.523 Å. Meanwhile, a longer P(1)–O(2) bond with a length of 1.557 Å can be found along the triad axis. All the P–O bond lengths are within a reasonable range (Fig. S2†).

In addition, there is one unique crystallographic Sn atom that coordinates with O(1), O(2) and two F(1) atoms to form a distorted $[SnO_2F_2]^{4-}$ tetrahedron in $[Sn_3F_3]PO_4$ (Fig. 1c). In the $[SnO_2F_2]^{4-}$ tetrahedron, the lengths of Sn–O bonds are 2.098 and 2.567 Å and Sn–F bonds are 2.058 and 2.264 Å within a reasonable bond length range. Furthermore, each $[SnO_2F_2]^{4-}$ tetrahedron is linked with the adjacent one by a shared F atom to form a 3_1 counterclockwise spiral chain $[SnO_2F]^{3-}_\infty$ which is along the c direction (Fig. 1a). The spiral chains are connected by shared O atoms to form a 3D network structure, within which the $[PO_4]^{3-}$ tetrahedra are incorporated. Observing this structure, a hole with a diameter of 2.35 Å can be found. However, it's smaller than the diameter 2.75 Å of a H_2O molecule reported in the literature,[40] and it's assumed that the H_2O molecule couldn't be filled in. This observation is in line with the experimental result that regardless of changing the experimental conditions, the crystalline hydrate of $[Sn_3F_3]PO_4$ can't be obtained.

Besides, the $[Sn_3OF]PO_4$ compound can be transformed from the $[Sn_3F_3]PO_4$ compound by substituting two F$^-$ with one O^{2-}. To be specific, the change in the crystal structure begins with the conversion from the $[Sn_3O_4F_6]^{8-}$ polyhedron in $[Sn_3F_3]PO_4$ to the $[Sn_3O_6F_2]^{8-}$ polyhedron in $[Sn_3OF]PO_4$. As shown in Fig. 1c, the three same $[SnO_2F_2]^{4-}$ polyhedra in the $[Sn_3F_3]PO_4$ compound form a $[Sn_3O_4F_6]^{8-}$ trimer by sharing the O(2) atom. Moreover, it is found that the $[Sn_3O_4F_6]^{8-}$ polyhedron is similar to the $[Sn_3O_6F_2]^{8-}$ polyhedron in the $[Sn_3OF]PO_4$ compound. Therefore, what can force the structure transformation? Actually, as illustrated in Fig. 1c and f, a $[SnO_2F_2]^{4-}$ polyhedron remains and the other two $[SnO_2F_2]^{4-}$ polyhedra rotate along the Sn(1)–O(2) bonds. The rotation ultimately leads to a change in the polyhedral structure from $[Sn_3O_4F_6]^{8-}$ in $[Sn_3F_3]PO_4$ to $[Sn_3O_6F_2]^{8-}$ in $[Sn_3OF]PO_4$. Then, through the substitution of O and F atoms, the transformation can be achieved.

Herein, $[Sn_3O_6F_2]^{8-}$ as the Sn-centered structure framework unit forms a $[Sn_3O_5F]^{5-}_\infty$ 2D layer (Fig. 1e) through the edge-sharing O(1) atom along the b direction and the corner-sharing F(1) atom along the c direction. Linked with the $[PO_4]^{3-}$ tetrahedra along the a direction, the adjacent layers are connected to form a 3D $[Sn_3OF]PO_4$ network structure (Fig. 1d). In $[Sn_3OF]PO_4$, each crystallographic symmetric unit

5650 | *Inorg. Chem. Front.*, 2024, **11**, 5648–5656

This journal is © the Partner Organisations 2024

Fig. 1 The structures of $[Sn_3F_3]PO_4$ and $[Sn_3OF]PO_4F$. Tin: gray, phosphorus: dark blue, oxygen: red, fluorine: dusty blue, and $[PO_4]^{3-}$ dusty blue. (a) The spiral chain $[SnO_2F]_\infty^{3-}$. (b) The 3D structure of $[Sn_3F_3]PO_4$. (c) The $[Sn_3O_4F_6]^{8-}$ polyhedron with the attached $[PO_4]^{3-}$. (d) The 3D structure of $[Sn_3OF]PO_4F$. (e) The $[Sn_3O_5F]_\infty^{5-}$ layer. (f) $[Sn_3O_6F_2]^{8-}$.

consists of three unique 4e sites occupied by Sn, one unique 4e site occupied by P, five unique 4e sites occupied by O and one unique 4e site occupied by F. All the bonds are within a reasonable range, of which the Sn–O bond is from 2.067 Å to 2.740 Å, the Sn–F bond is from 2.259 Å to 2.283 Å and the P–O bond is from 1.532 Å to 1.559 Å (Fig. 1f and S2†).

Because of the transformation of the crystal structure from $[Sn_3F_3]PO_4$ to $[Sn_3OF]PO_4$, the space group changes from $R3$ to $P2_1/c$, that is to say, from a high symmetry to a low symmetry. What causes it? From Fig. 2a viewed along the ab plane, it can be observed that the $[Sn_3F_3]PO_4$ compound has two kinds of symmetric axes, C_3 and 3_1 axes. For instance, the $[PO_4]^{3-}$ polyhedron is located on the C_3 axis, and the $[SnO_2F]_\infty^{3-}$ chain is parallel to the 3_1 axis. However, due to the abovementioned rotation (Sn(1)–O(2)) in Sn-centered structure framework units and the assistance from the O atom which results in asymmetric components from $[Sn_3F_3]PO_4$ to $[Sn_3OF]PO_4$, the higher symmetric 3_1 and C_3 axes are destroyed, resulting in a transformation from a high symmetry ($R3$) to a low symmetry ($P2_1/c$).

Optical and thermal properties

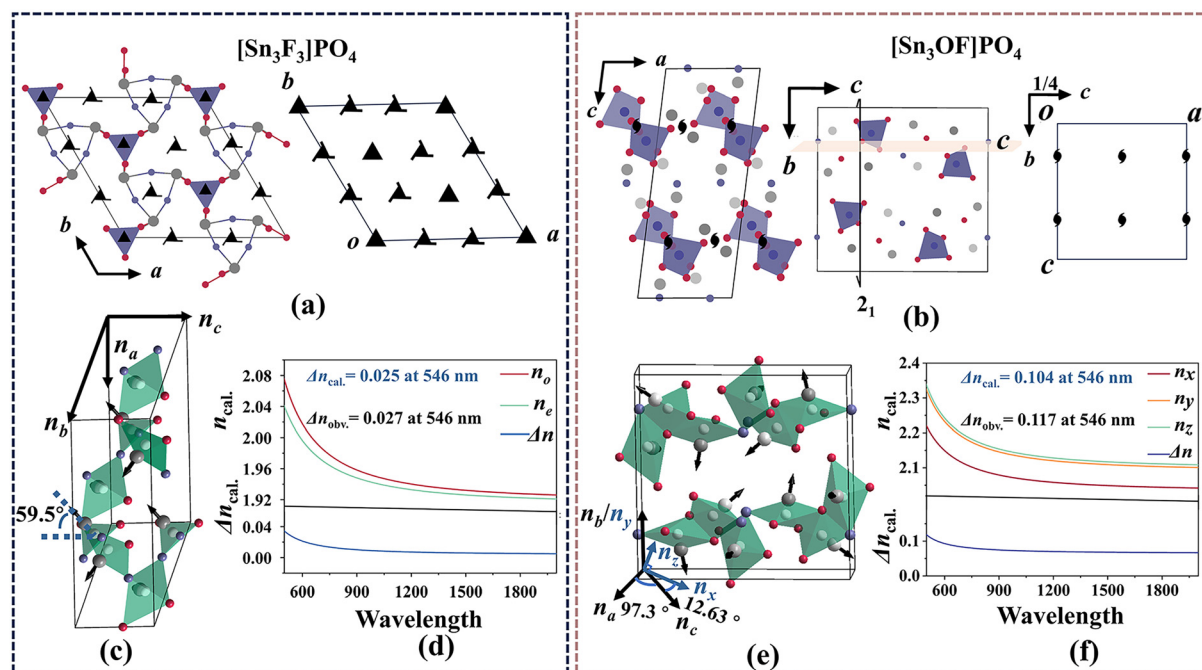The UV/Vis-NIR diffuse reflection spectrum was obtained and is shown in Fig. S3.† It presents the UV cutoff edges of $[Sn_3F_3]PO_4$ and $[Sn_3OF]PO_4$, which are 258 nm and 306 nm, respectively. The converted absorption pattern indicates that the corresponding band gaps of $[Sn_3F_3]PO_4$ and $[Sn_3OF]PO_4$ are 4.31 eV and 3.62 eV, respectively, and the distinction derives from that $[Sn_3F_3]PO_4$ has more F atoms that are more electronegative than the O atom.[41]

Combining the IR absorption spectrum in Fig. S4,† it could be indicated that 1058, 997, and 940 cm^{-1} for $[Sn_3F_3]PO_4$ and 1039, 981, and 948 cm^{-1} for $[Sn_3OF]PO_4$ are from the asymmetric stretching vibrations of $[PO_4]^{3-}$ groups, while 586 and 555 cm^{-1} for $[Sn_3F_3]PO_4$ and 610, 579, and 533 cm^{-1} for $[Sn_3OF]PO_4$ are from the asymmetric bending vibrations of $[PO_4]^{3-}$ groups. This demonstrates that there are $[PO_4]^{3-}$ groups in the title compounds.

The second harmonic generation (SHG) signal of $[Sn_3F_3]$ PO_4 at a 1064 nm light source with a different particle size is shown in Fig. S5.† The result illustrates that $[Sn_3F_3]PO_4$ is phase-matchable at 1064 nm and features a weak SHG response, about 0.3 × KDP. Besides, energy dispersive spectroscopy (EDS) confirmed the existence of Sn, P, O and F elements in both $[Sn_3F_3]PO_4$ and $[Sn_3OF]PO_4$ (Fig. S6†). The thermogravimetric analysis (TG) and differential scanning calorimetry (DSC) curves indicated that $[Sn_3F_3]PO_4$ and $[Sn_3OF]PO_4$ are relatively stable before 300 °C and gradually decompose after that (Fig. S7†).

In addition, for linear optical properties of $[Sn_3F_3]PO_4$ and $[Sn_3OF]PO_4$, according to crystal thicknesses d (38.6 and

This journal is © the Partner Organisations 2024

Inorg. Chem. Front., 2024, **11**, 5648–5656 | **5651**

Fig. 2 (a) $[Sn_3F_3]PO_4$ viewed along the *ab* plane and the [001] projection of the symmetry elements of the space group *R*3. (b) $[Sn_3OF]PO_4F$ viewed along the *ac* and *bc* planes and the [010] projection of the symmetry elements of the space group $P2_1/c$. (c and e) The orientation of Sn-based polyhedra in $[Sn_3F_3]PO_4$ and $[Sn_3OF]PO_4F$, respectively. (d and f) The calculated birefringence and the observed birefringence at 546 nm for $[Sn_3F_3]PO_4$ and $[Sn_3OF]PO_4F$, respectively.

31.0 μm, respectively) and delay values for full extinction *R* at 546 nm (1.06 and 3.62 μm, respectively) (Fig. S8†), the birefringences of $[Sn_3F_3]PO_4$ and $[Sn_3OF]PO_4$ are larger than 0.027 and 0.117 at 546 nm based on formula (1), respectively. The birefringence of $[Sn_3OF]PO_4$ exceeds that of many tin(II) phosphates, such as $Sn_3(PO_4)_2$ (0.052 at 1064 nm), $Rb(Sn_3O)_2(PO_4)_3$ (0.081 at 1064 nm), and $NH_4(Sn_3O)_2(PO_4)_3$ (0.082 at 1064 nm). Moreover, the calculated birefringences of $[Sn_3F_3]PO_4$ and $[Sn_3OF]PO_4$ are 0.025 and 0.104 at 546 nm, respectively, which are in good agreement with the experimental data (Fig. 2d and f). Furthermore, the birefringence of $[Sn_3OF]PO_4$ is almost five times that of $[Sn_3F_3]PO_4$. But why is the optical anisotropy so different for the title compounds that contain the same element and why is there such a large birefringence gain?

Origin of birefringence

Generally speaking, a rigid tetrahedron, such as $[PO_4]^{3-}$, with small polarizability anisotropy contributes little to birefringence.[42–44] Hence, the optical anisotropy of $[Sn_3F_3]PO_4$ and $[Sn_3OF]PO_4$ mainly hinges on the geometry of the asymmetric Sn-centered polyhedron ($[SnO_2F_2]^{4-}$ for $[Sn_3F_3]PO_4$ and $[SnO_3F]^{5-}$ for $[Sn_3OF]PO_4$) with stereochemically active lone pairs as well as the orientation. The orientation of lone pairs is consistent with the direction from the center of the polyhedron ($[SnO_2F_2]^{4-}$ in $[Sn_3F_3]PO_4$ and $[SnO_3F]^{5-}$ in $[Sn_3OF]PO_4$) to the Sn atom (Fig. 2c and e).[45] In fact, optical anisotropy originates from the different contributions of stereochemically active lone pairs towards the dielectric axis. Large contribution differences often correspond to large optical anisotropy.

On the one hand, since the $[Sn_3F_3]PO_4$ compound crystallizes in the higher symmetric space group *R*3, there are angles of 59.3° between all the lone pairs in Sn-centered polyhedra and the *c*-axis in the unit cell (Fig. 2c). Then the orientation of the lone pairs in Sn-based polyhedra can be projected on the *ac* plane and perpendicular to the *ac* plane, respectively. It is speculated that if the angle is 45° between the lone pairs and the *c*-axis, it can result in minimum anisotropy because there are the two approximate contributions of stereochemically active lone pairs to the optical anisotropy along the *ac* plane and perpendicular to the *ac* plane. Consequently, the contributions of stereochemically active lone pairs of $[SnO_2F_2]^{4-}$ in $[Sn_3F_3]PO_4$ to the optical anisotropy along the *ac* plane and perpendicular to the *ac* plane are 5.46 and 4.29, respectively (detailed calculations are provided in Table S4†). Therefore, it demonstrates that there is a little difference in the contribution, which results in small optical anisotropy.

On the other hand, $[Sn_3OF]PO_4$ belongs to a lower symmetry ($P2_1/c$), and the dielectric axes are shown in Fig. 2e. The contributions of three unique crystallographic Sn-based polyhedra in $[Sn_3OF]PO_4$ are different, as for $[Sn(1)O_3F]^{5-}$: 0.56, 0.48, and 3.44, $[Sn(2)O_3F]^{5-}$: 0.16, 3.44, and 0.60, and $[Sn(3)O_3F]^{5-}$: 2.08, 2.24, and 2.20 along the dielectric axis (n_x, n_y, and n_z), respectively. Compared with Sn(3), $[Sn(1)O_3F]^{5-}$ and $[Sn(2)O_3F]^{5-}$ have a greater distinction in contributions on the three axes, and it could be inferred that Sn(1) and Sn(2) may have a greater effect on optical anisotropy. At the same time, the total contributions are 2.80, 6.16 and 6.24 along the dielec-

5652 | *Inorg. Chem. Front.*, 2024, **11**, 5648–5656

This journal is © the Partner Organisations 2024

tric axis (n_x, n_y, and n_z), respectively (detailed calculations are provided in Table S4†). This agrees well with the relationship among the calculated refractive indices n_x, n_y and n_z, where n_z and n_y are far larger than n_x. Hence, a relatively large difference in the contribution drives large optical anisotropy, agreeing with the experimental birefringence.
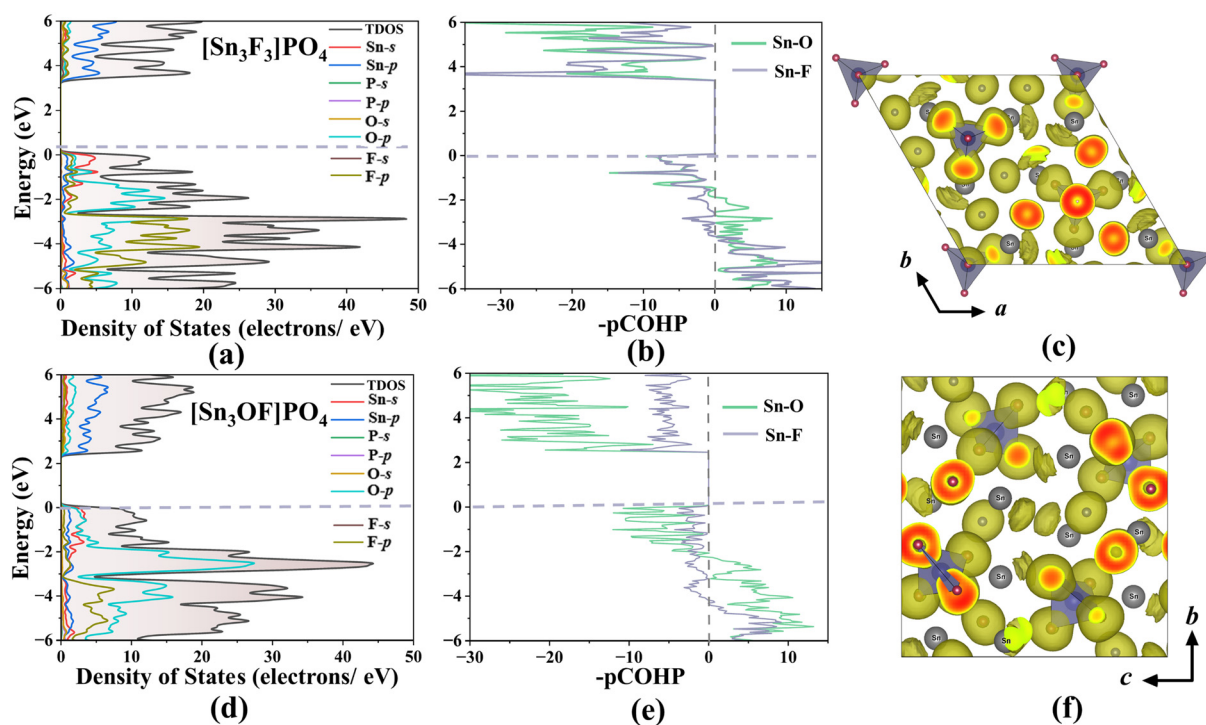
Additionally, considering the aligned cooperativity of the asymmetric Sn-centered polyhedron, defined $\frac{\sum_i^n \cos \theta_i}{n}$ (θ_i represents the ith angle between the polyhedra; n represents the number of angles per unit),[45] it is observed that asymmetric Sn-centered polyhedra in [Sn$_3$OF]PO$_4$ have more aligned cooperativity than those in [Sn$_3$F$_3$]PO$_4$ (0.54 *vs.* 0.47) (detailed calculations are provided in Tables S4 and S5†).

Thus, it can be inferred that a large birefringence enhancement is achieved by breaking the symmetry with disadvantage for optical anisotropy and reconstructing the aligned arrangement of the lone pairs. Combined with the above view, the explanation is represented for KSn$_4$(PO$_4$)$_3$ (*R3c*, 0.013 at 1064 nm) and NaSn$_4$(PO$_4$)$_3$ (*R3c*, 0.005 at 1064 nm) with high symmetry and small birefringence. The reason is that [SnO$_3$]$^{4-}$ polyhedra in the two isostructural compounds, Sn-centered structure framework units, are coincidentally located on the *C*3 and 3$_1$ axes, as shown in Fig. S9.† It results in a small distinction in contributions of optical anisotropy.

Theoretical calculations

Both the geometric configuration and electronic structure are significant factors affecting the optical properties. The partial density of states (PDOS) of [Sn$_3$F$_3$]PO$_4$ and [Sn$_3$OF]PO$_4$ are illustrated in Fig. 3(a) and (d), respectively. For both [Sn$_3$F$_3$]PO$_4$ and [Sn$_3$OF]PO$_4$, the CBM (Conduction Band Minimum) is mainly composed of the 5*p* states of Sn atoms, while the VBM (Valence Band Maximum) is mainly composed of the 5*s* states of Sn atoms and the 2*p* states of O atoms. However, the contribution of O-2*p* states around the VBM in [Sn$_3$OF]PO$_4$ is larger than that in [Sn$_3$F$_3$]PO$_4$. This is consistent with the larger band gap of [Sn$_3$F$_3$]PO$_4$ (band gaps calculated using PBE are shown in Fig. S10†). To deeply understand the bonding feature of [Sn$_3$F$_3$]PO$_4$ and [Sn$_3$OF]PO$_4$, the negative partial crystal orbital Hamiltonian population[46–48] (pCOHP) is presented in Fig. 3(b) and (e). Below the Fermi level, a partition of the valence states appears as antibonding states for both Sn–O and Sn–F bonds. However, the antibonding interactions in [Sn$_3$F$_3$]PO$_4$ are smaller than those in [Sn$_3$OF]PO$_4$. Thus, the Sn–O and Sn–F bonds in [Sn$_3$F$_3$]PO$_4$ are stronger than those in [Sn$_3$OF]PO$_4$. Furthermore, it can be visualized from the electron localization function (ELF) diagrams (Fig. 3c and f) that Sn^{2+} has an asymmetric cloud of lone pairs, indicating that both [Sn$_3$F$_3$]PO$_4$ and [Sn$_3$OF]PO$_4$ show considerable strength of lone pairs under the same conditions. Therefore, there is no obvious difference in the electronic structure compared to the large observed birefringence difference between [Sn$_3$F$_3$]PO$_4$ and [Sn$_3$OF]PO$_4$. Therefore, the effect of the electronic structure on birefringence is relatively small. Hence, it can be inferred that the geometries rather than electronic structures play an important role in contributing to the optical properties.

Fig. 3 (a and d) Partial density of states (PDOS), (b and e) negative crystal orbital Hamiltonian population (−pCOHP), and (c and f) electron localization function (ELF) diagrams of [Sn$_3$F$_3$]PO$_4$ and [Sn$_3$OF]PO$_4$, respectively.

This journal is © the Partner Organisations 2024

Inorg. Chem. Front., 2024, **11**, 5648–5656 | **5653**

Conclusions

In conclusion, a novel compound $[Sn_3OF]PO_4$ is discovered, exhibiting significant birefringence ($\Delta n_{obv.}$ = 0.117 at 546 nm), a five-fold improvement compared to that of a related compound $[Sn_3F_3]PO_4$. The remarkable enhancement in birefringence is primarily attributed to the anisotropic $[SnO_3F]^{5-}$ structure building unit. By simple regulation of the F/O ratio, the undesirable $R3$ symmetry in $[Sn_3F_3]PO_4$ is disrupted. This regulation also realigns the lone pairs, resulting in substantial optical anisotropy. These strategies for designing compounds and optimizing performance could serve as an experimental guideline for discovering and optimizing effective birefringent crystals.

Author contributions

Y. H. H., J. Y. G. and L. M. W. conceived, designed and performed all the experimental work. X. X. and J. Y. H. performed the theoretical calculations. Y. H. H. and L. C. wrote the draft paper. All the authors discussed the results and commented on the manuscript. All authors contributed to the general discussion.

Data availability

The data supporting this article have been included as part of the ESI.†

Crystallographic data have been deposited at CCDC 2332572 and 2334179 for $[Sn_3OF]PO_4$ and $[Sn_3F_3]PO_4$, respectively.†

Conflicts of interest

There are no conflicts to declare.

Acknowledgements

References

1 S. J. Han, A. Tudi, W. B. Zhang, X. L. Hou, Z. H. Yang and S. L. Pan, Recent development of Sn[II], Sb[III]-based birefringent material: crystal chemistry and investigation of birefringence, *Angew. Chem., Int. Ed.*, 2023, **62**, e202302025.

2 K. M. Ok, Toward the rational design of novel noncentrosymmetric materials: factors influencing the framework structures, *Acc. Chem. Res.*, 2016, **49**, 2774–2785.

3 C. Wu, X. X. Jiang, Z. J. Wang, L. Lin, Z. S. Lin, Z. P. Huang, X. F. Long, M. G. Humphrey and C. Zhang, Giant optical anisotropy in the UV-transparent 2D nonlinear optical material $Sc(IO_3)_2(NO_3)$, *Angew. Chem., Int. Ed.*, 2021, **60**, 3464–3468.

4 X. D. Chai, M. Z. Li, S. J. Lin, W. F. Chen, X. M. Jiang, B. W. Liu and G. C. Guo, $Cs_4Zn_5P_6S_{18}I_2$: the largest birefringence in chalcohalide achieved by highly polarizable nonlinear optical functional motifs, *Small*, 2023, **19**, 2303847.

5 Y. Lin, C. L. Hu, Z. Fang, J. Chen, W. J. Xie, Y. Chen, J. P. Wang and J. G. Mao, $KRE(CO_3)_2$ (RE = Eu, Gd, Tb): new mixed metal carbonates with strong photoluminescence and large birefringence, *Inorg. Chem. Front.*, 2022, **9**, 5645–5652.

6 G. Q. Zhou, J. Xu, X. D. Chen, H. Y. Zhong, S. T. Wang, K. Xu, P. Z. Deng and F. X. Gan, Growth and spectrum of a novel birefringent α-BaB_2O_4 crystal, *J. Cryst. Growth*, 1998, **191**, 517–519.

7 A. Tudi, S. J. Han, Z. H. Yang and S. L. Pan, Potential optical functional crystals with large birefringence: recent advances and future prospects, *Coord. Chem. Rev.*, 2022, **459**, 214380.

8 J. Lu, Y. K. Lian, L. Xiong, Q. R. Wu, M. Zhao, K. X. Shi, L. Chen and L.-M. Wu, How to maximize birefringence and nonlinearity of π-conjugated cyanurates, *J. Am. Chem. Soc.*, 2019, **141**, 16151–16159.

9 X. Liu, Y. C. Yang, M. Y. Li, L. Chen and L.-M. Wu, Anisotropic structure building unit involving diverse chemical bonds: a new opportunity for high-performance second-order NLO materials, *Chem. Soc. Rev.*, 2023, **52**, 8699–8720.

10 G. Q. Shi, Y. Wang, F. F. Zhang, B. B. Zhang, Z. H. Yang, X. L. Hou, S. L. Pan and K. R. Poeppelmeier, Finding the next deep-ultraviolet nonlinear optical material: $NH_4B_4O_6F$, *J. Am. Chem. Soc.*, 2017, **139**, 10645–10648.

11 S. J. Han, B. B. Zhang, Z. H. Yang and S. L. Pan, From LiB_3O_5 to $NaRbB_6O_9F_2$: fluorine-directed evolution of structural chemistry, *Chem. – Eur. J.*, 2018, **24**, 10022–10027.

12 J. Lu, J. N. Yue, L. Xiong, W. K. Zhang, L. Chen and L.-M. Wu, Uniform alignment of non-π-conjugated species enhances deep ultraviolet optical nonlinearity, *J. Am. Chem. Soc.*, 2019, **141**, 8093–8097.

13 S. J. Han, M. Mutailipu, A. Tudi, Z. H. Yang and S. L. Pan, $PbB_5O_7F_3$: a high-performing short-wavelength nonlinear optical material, *Chem. Mater.*, 2020, **32**, 2172–2179.

14 M. Mutailipu, M. Zhang, B. B. Zhang, L. Y. Wang, Z. H. Yang, X. Zhou and S. L. Pan, $SrB_5O_7F_3$ functionalized with $[B_5O_9F_3]^{6-}$ chromophores: accelerating the rational design of deep-ultraviolet nonlinear optical materials, *Angew. Chem., Int. Ed.*, 2018, **57**, 6095–6099.

15 M. Mutailipu, J. Han, Z. Li, F. M. Li, J. J. Li, F. F. Zhang, X. F. Long, Z. H. Yang and S. L. Pan, Achieving the full-wavelength phase-matching for efficient nonlinear optical

5654 | *Inorg. Chem. Front.*, 2024, **11**, 5648–5656

This journal is © the Partner Organisations 2024

frequency conversion in $C(NH_2)_3BF_4$, *Nat. Photonics*, 2023, **17**, 694–701.

16 Y. Wang, B. B. Zhang, Z. H. Yang and S. L. Pan, Cation-tuned synthesis of fluorooxoborates: towards optimal deep-ultraviolet nonlinear optical materials, *Angew. Chem., Int. Ed.*, 2018, **57**, 2150–2154.

17 B. B. Zhang, G. P. Han, Y. Wang, X. L. Chen, Z. H. Yang and S. L. Pan, Expanding frontiers of ultraviolet nonlinear optical materials with fluorophosphates, *Chem. Mater.*, 2018, **30**, 5397–5403.

18 L. Xiong, J. Chen, J. Lu, C.-Y. Pan and L.-M. Wu, Monofluorophosphates: a new source of deep-ultraviolet nonlinear optical materials, *Chem. Mater.*, 2018, **30**, 7823–7830.

19 Y. Yang, Y. Qiu, P. F. Gong, L. Kang, G. M. Song, X. M. Liu, J. L. Sun and Z. S. Lin, Lone-Pair enhanced birefringence in an alkaline-earth metal tin(II) phosphate $BaSn_2(PO_4)_2$, *Chem. – Eur. J.*, 2019, **25**, 5648–5651.

20 J. Y. Guo, A. Tudi, S. J. Han, Z. H. Yang and S. L. Pan, $Sn_2B_5O_9Cl$: a material with large birefringence enhancement activated prepared via alkaline-earth-metal substitution by tin, *Angew. Chem., Int. Ed.*, 2019, **58**, 17675–17678.

21 Y. C. Liu, X. M. Liu, S. Liu, Q. R. Ding, Y. Q. Li, L. N. Li, S. G. Zhao, Z. S. Lin, J. H. Luo and M. C. Hong, An unprecedented antimony(III) borate with strong linear and nonlinear optical responses, *Angew. Chem., Int. Ed.*, 2020, **59**, 7793–7796.

22 J. Y. Guo, A. Tudi, S. J. Han, Z. H. Yang and S. L. Pan, α-SnF_2: a UV birefringent material with large birefringence and easy crystal growth, *Angew. Chem., Int. Ed.*, 2021, **60**, 3540–3544.

23 J. Y. Guo, S. C. Cheng, S. J. Han, Z. H. Yang and S. L. Pan, $Sn_2B_5O_9Br$ as an outstanding bifunctional material with strong second-harmonic generation effect and large birefringence, *Adv. Opt. Mater.*, 2021, **9**, 2001734.

24 J. Y. Guo, A. Tudi, S. J. Han, Z. H. Yang and S. L. Pan, Sn_2PO_4I: an excellent birefringent material with giant optical anisotropy in non π-conjugated phosphate, *Angew. Chem., Int. Ed.*, 2021, **60**, 24901–24904.

25 J. F. Deng, Y. J. Kang, J. X. Mi, M. R. Li, J. T. Zhao and S. Y. Mao, $KSn_4(PO_4)_3$, *Acta Crystallogr.*, 2004, **60**, i116–i117.

26 S. Y. Mao, J. F. Deng, M. R. Li, J. X. Mi, H. H. Chen and J. T. Zhao, Crystal structure of sodium tetratin(II) triphosphate, $NaSn_4(PO_4)_3$, *Z. Kristallogr. – New Cryst. Struct.*, 2004, **219**, 205–206.

27 S. B. Etcheverry, G. E. Narda, M. C. Apella and E. J. Baran, Hydrolytic properties of $Sn_3PO_4F_3$ (short communication), *Caries Res.*, 1986, **20**, 120–122.

28 P. Yu, L.-M. Wu, L. J. Zhou and L. Chen, Deep-ultraviolet nonlinear optical crystals: $Ba_3P_3O_{10}X$ (X = Cl, Br), *J. Am. Chem. Soc.*, 2014, **136**, 480–487.

29 H. W. Yu, W. G. Zhang, J. Young, J. M. Rondinelli and P. S. Halasyamani, Design and synthesis of the beryllium-free deep-ultraviolet nonlinear optical material $Ba_3(ZnB_5O_{10})PO_4$, *Adv. Mater.*, 2015, **27**, 7380–7385.

30 J. Chen, L. Xiong, L. Chen and L.-M. Wu, $Ba_2NaClP_2O_7$: unprecedented phase matchability induced by symmetry breaking and its unique fresnoite-type structure, *J. Am. Chem. Soc.*, 2018, **140**, 14082–14086.

31 SAINT, *version 7.60A*, Bruker Analytical X-ray Instruments, Inc., Madison, WI, 2013.

32 SHELXTL, *version 6.1*, Bruker Analytical X-ray Instruments, Inc., Madison, WI, 2013.

33 P. Kubelka and F. Munk, An article on optics of paint layers, *Tech. Phys.*, 1931, **12**, 593–609.

34 P. Hohenberg and W. Kohn, Density functional theory (DFT), *Phys. Rev.*, 1964, **136**, B864–B871.

35 W. Kohn and L. J. Sham, Self-consistent equations including exchange and correlation effects, *Phys. Rev.*, 1965, **140**, A1133–A1138.

36 G. Kresse and J. Hafner, Ab initio molecular dynamics for liquid metals, *Phys. Rev. B: Condens. Matter Mater. Phys.*, 1993, **47**, 558–561.

37 G. Kresse and J. Furthmüller, Efficient iterative schemes for ab initio total-energy calculations using a plane-wave basis set, *Phys. Rev. B: Condens. Matter Mater. Phys.*, 1996, **54**, 11169–11186.

38 J. P. Perdew, K. A. Jackson, M. R. Pederson, D. J. Singh and C. Fiolhais, Erratum: atoms, molecules, solids, and surfaces: applications of the generalized gradient approximation for exchange and correlation, *Phys. Rev. B: Condens. Matter Mater. Phys.*, 1993, **46**, 4978.

39 J. P. Perdew, K. Burke and M. Ernzerhof, Generalized gradient approximation made simple, *Phys. Rev. Lett.*, 1996, **77**, 3865–3868.

40 M. Caurie, The unimolecular character of the classical Brunauer, Emmett and Teller adsorption equation and moisture adsorption, *Int. J. Food Sci. Technol.*, 2005, **40**, 283–293.

41 W. Q. Jin, C. W. Xie, X. L. Hou, M. Cheng, E. Tikhonov, M. F. Wu, S. L. Pan and Z. H. Yang, From monofluorophosphates A_2PO_3F to difluorophosphates APO_2F_2 (A = alkali metal): design of new potential deep-ultraviolet nonlinear optical system with shortened phase-matching wavelength, *Chem. Mater.*, 2023, **35**, 5281–5290.

42 X. H. Zhang, B. P. Yang, J. Chen, C. L. Hu, Z. Fang, Z. J. Wang and J. G. Mao, A new iodate-phosphate $Pb_2(IO_3)(PO_4)$ achieving great improvement in birefringence activated by $(IO_3)^-$ groups, *Chem. Commun.*, 2020, **56**, 635–638.

43 L. Xiong, L.-M. Wu and L. Chen, A general principle for DUV NLO materials: π-conjugated confinement enlarges band gap, *Angew. Chem., Int. Ed.*, 2021, **60**, 25063–25067.

44 X. Y. Zhang, L. Kang, P. F. Gong, Z. S. Lin and Y. C. Wu, Nonlinear optical oxythiophosphate approaching the good balance with wide ultraviolet transparency, strong second harmonic effect, and large birefringence, *Angew. Chem., Int. Ed.*, 2021, **60**, 6386–6390.

45 J. Y. Guo, J. B. Huang, A. Tudi, X. L. Hou, S. J. Han, Z. H. Yang and S. L. Pan, Birefringence regulation by clari-

This journal is © the Partner Organisations 2024

Inorg. Chem. Front., 2024, **11**, 5648–5656 | **5655**

fying the relationship between stereochemically active lone pairs and optical anisotropy in tin-based ternary halides, *Angew. Chem., Int. Ed.*, 2023, **62**, e202304238.

46 A. Walsh and G. W. Watson, Influence of the anion on lone pair formation in Sn(II) monochalcogenides: a DFT study, *J. Phys. Chem. B*, 2005, **109**, 18868–18875.

47 A. Walsh, D. J. Payne, R. G. Egdell and G. W. Watson, Stereochemistry of post-transition metal oxides: revision of the classical lone pair model, *Chem. Soc. Rev.*, 2011, **40**, 4455–4463.

48 V. L. Deringer, A. L. Tchougréeff and R. Dronskowski, Crystal orbital hamilton population (COHP) analysis as projected from plane-wave basis sets, *J. Phys. Chem. A*, 2011, **115**, 5461–5466.

5656 | *Inorg. Chem. Front.*, 2024, **11**, 5648–5656

This journal is © the Partner Organisations 2024